48th AIAA/ASME/SAE/ASEE Joint Propulsion Conference & Exhibit
30 July - 01 August 2012, Atlanta, Georgia

AIAA 2012-4117

Hall Effect Thruster Plasma Plume Characterization with Probe Measurements and Self-Similar Fluid Models

K. Dannenmayer* and S. Mazouffre†
ICARE - CNRS, Orléans 45071 France

M. Merino‡ and E. Ahedo§
Universidad Politécnica de Madrid, Madrid 28040 Spain

A characterization of the far-field plasma plume of two Hall effect thrusters was performed by means of a comparison between experimental plasma properties with semi-analytical fluid models of the hypersonic plasma plume. A cylindrical Langmuir probe was employed in the experimental investigation of the plumes. Time-averaged measurements of the plasma potential, the electron temperature and density were performed for various operating conditions of the PPS®100-ML and the PPI thruster. The measured data was then used to fit a simple fluid model that relies on the quasi-selfsimilarity exhibited by hypersonic plasma plumes. Model agrees well with experimental data and the error committed by the selfsimilarity assumption is shown to be small.

Nomenclature

CRP	Cathode-to-ground potential [V]
I_d	Discharge current [A]
n	Plasma density [m^{-3}]
T_e	Electron temperature [eV]
U_d	Discharge voltage [V]
ϕ	Plasma potential [V]
u_{zi}, u_{ri}	Axial and radial ion velocity components [m/s]
γ	Specific heat ratio of electrons

I. Introduction

Electric propulsion is at present a well established technology for space applications. In comparison with chemical rockets, electric propulsion devices offer an attractive way to save propellant mass thanks to a much faster propellant ejection speed. Among all electric propulsion devices, Hall effect thrusters (HET) are currently recognized as an attractive propulsion means for long duration missions and maneuvers that require a large velocity increments. A HET uses a low-pressure discharge with magnetized electrons to ionize and accelerate a propellant gas.[1]

The plasma plume of a HET exhibits a relatively large divergence angle of about 45° (Ref. 2). The characterization and the investigation of the plume and its expansion into space is therefore paramount for understanding these devices and assessing the mechanical and electrical interactions of the exhaust plasma plume with the spacecraft itself and the surrounding environment.[3,4] Furthermore, understanding the dependence of the plume evolution with the main operating parameters allows to (1) optimize thruster design for maximum performance, (2) reduce potential interaction hazards, and (3) produce a tailored plasma

*PhD student (kathe.dannenmayer@cnrs-orleans.fr).
†Research scientist, Electric propulsion team leader (stephane.mazouffre@cnrs-orleans.fr).
‡PhD student, Equipo de Propulsión Espacial y Plasmas (EP2, web.fmetsia.upm.es/ep2), student AIAA member (mario.merino@upm.es).
§Professor, EP2, senior AIAA member (eduardo.ahedo@upm.es).

jet for advanced applications, such as the recently introduced Ion Beam Shepherd system, a contactless space "tow" system, which employs an energetic plasma plume to exert a force on a distant object.[5]

Analysis of electric propulsion plasma plumes constitutes a difficult task, due to the complexity and number of phenomena taking place in the plume formation and downstream expansion. Usually, a triple approach combining ground testing, in-space measurements and modeling must be followed to correctly describe the plume. The present work is focused on the study and characterization of the plasma plumes generated by two different HETs. Experimental data for plasma properties, such as plasma potential, electron temperature and density, are obtained using a cylindrical probe. Semi-analytical, selfsimilar fluid models of the hypersonic far-field plasma plume are then used to fit and assimilate the experimental data from the probe, in order to recover features such as the shape of ion streamtubes.

The rest of the paper is organized as follows. Section II details the experimental setup for the two HETs, the PPS®100-ML and the PPI thruster. Section III presents the experimental results. The self-similar model and its fitting to the measured plume data is performed in section IV. Conclusions of this work are summarized in the final section.

II. Experimental setup

Electrostatic probes are a simple and versatile diagnostic tool for the experimental investigation of plasma properties. In the present work, a single cylindrical Langmuir probe was used to investigate the electron properties in the far-field plumes of the two HETs, namely the 1.5 kW PPS®100-ML and the 200 W PPI thruster. A detailed description and analysis of the probe is given in a previous paper.[6] A brief summary of the thrusters and the experimental setup is given in the following.

II.A. PPS®100-ML

The PPS®100-ML is a 1.5 kW-class HET with a discharge chamber outer diameter of 100 mm (Ref. 7). The magnetic field is generated by 5 magnetic coils (4 external and 1 internal coil). The thruster delivers a thrust of about 80 mN when operated at 300 V and 5 mg/s. The channel walls are made of $BNSiO_2$. A picture of the PPS®100-ML thruster is shown in Figure 1. The thruster was operated in the PIVOINE-2G

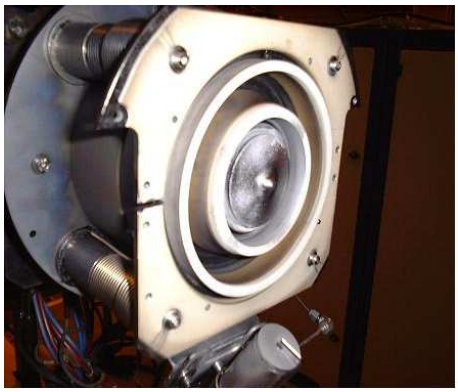

Figure 1. Picture of the PPS®100-ML.

(**P**ropulsion **I**onique pour les **V**ols **O**rbitaux – **I**nterprétation et **N**ouvelles **E**xpériences; 2G stands for 2nd generation) chamber. The test bench is a 4 m long by 2.2 m in diameter vacuum chamber equipped with cryogenic pumps. It has a maximum pumping speed in xenon of 210 000 l/s (40 K) providing a background pressure of about 10^{-5} mbar-Xe for a broad range of operating conditions (1-50 mg/s in Xe and a power range from 100 W up to 20 kW). The multi-stage pumping system is composed of a primary pump, a 5000 l/s turbomolecular pump, for removal of light molecular gases like hydrogen and nitrogen that are not pumped by the cryosurfaces, as well as 2 cryogenic stages located at the back of the tank. The first stage allows to reach a pumping speed of 70 000 l/s. The second stage adds up a 140 000 l/s pumping capacity. In addition a 16 K cryo-panel is employed for removal of nitrogen and oxygen. The cryopumps are LN_2-cooled and shielded from ion beam by means of water-cooled graphite tiles. The tank pressure is measured with a cold cathode ionization gauge. The residual gas composition is continuously analyzed and monitored with a

quadrupole mass spectrometer. The thruster was mounted on a movable arm, allowing the displacement of the thruster along the thruster axis (x-direction). The diagnostics were mounted on a second arm that moves perpendicular to the thruster axis (y-direction). A rotation stage at the end of the diagnostics arm allowed a displacement of the probes in the θ- direction, so that the probes always pointed towards the thruster center, see Figure 2. The combination of the displacement of the probes in the y and θ-direction together with the possibility to move the thruster along its axis allowed to map the complete far-field plume. For the present study the far-field plume was mapped from 300 to 660 mm downstream the thruster exit plane and from 0 to 60 deg, where 0 deg corresponds to the thruster axis.

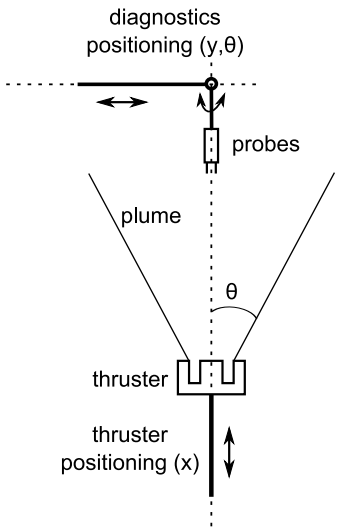

Figure 2. Schematic view of the HET and probe positioning system.

II.B. PPI thruster

The PPI thruster (French acronym for "**P**etit **P**ropulseur **I**nnovant") is a 200 W type HET able to deliver a thrust of 10 mN when operated at 250 V and 1.0 mg/s xenon mass flow rate.[8] This thruster was originally designed by the GEMaC team in Versailles.[9,10] This thruster exhibits three interesting features that makes it highly versatile. First, the magnetic field is generated by way of small SmCo magnets brought together inside rings located on either side of the channel walls. A soft iron magnetic circuit with a back gap permits to drive the magnetic flux in order to obtain the desired topology. No magnetic screen is used. Second, the propellant gas is injected homogeneously inside the channel using a porous ceramic instead of a classical metal hollow gas injector. A stainless-steel ring placed at the back of the channel serves as anode. Third, a central copper heat drain is employed to evacuate heat towards a radiator placed behind the thruster. The radiator, which is a thin copper disk of 25 cm in diameter, is necessary to reduce the thermal load onto dielectric walls and magnets. The channel walls are made of alumina compound (Al_2O_3). A heated cathode with a LaB_6 insert, provided by MIREA, is used with a cathode mass flow rate of 0.2 mg/s. A picture of the PPI thruster operating in the NExET test facility at 200 V and 1.0 mg/s is shown in Figure 3.

The thruster was operated in the NExET (**N**ew **EX**periments on **E**lectric **T**hrusters) test bench. This vacuum chamber has been installed at the ICARE laboratory in 2008. The stainless-steel vacuum chamber is 1.8 m long and 0.8 m in diameter. It is equipped with a multi-stage pumping system. This system is composed of a large dry pump (400 m^3/h), a 200 l/s turbomolecular pump to evacuate light gases and a cryogenic pump with a typical surface temperature of 35 K (8000 l/s) to get rid of the propellant such as xenon and krypton. A background pressure of 2×10^{-5} mbar is achieved with a xenon mass flow rate of 1.0 mg/s and an input power of 250 W (Ref. 11). The back part of the chamber is water cooled and protected with graphite tiles to absorb a part of the ion beam energy and therefore reducing the thermal load on the cryosurface. The chamber is equipped with different observation windows, diagnostic ports as well as electrical and gas feed-throughs. The interior of the test bench is easy to access thanks to a large front door. The thruster was mounted onto two moving stages to allow a displacement in both the axial (x) and radial (y) direction.

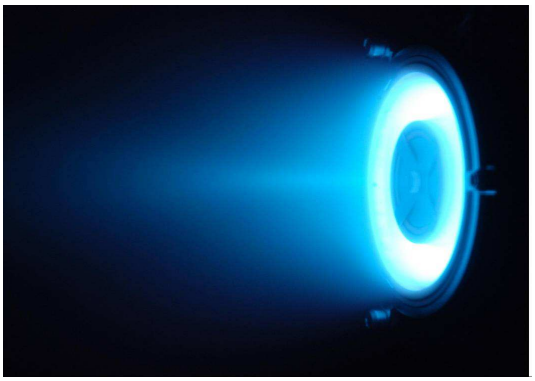

Figure 3. The 200 W-class PPI HET operating at 200 V and 1.0 mg/s in the NExET test bench (side view).

III. Experimental results

III.A. Far-field plume of the PPS®100-ML thruster

The PPS®100-ML was operated at a constant anode mass flow rate of 4.0 mg/s and cathode mass flow rate of 0.42 mg/s with three different discharge voltages (U_d =150, 200 and 300 V). Figure 4 shows the variation of ϕ, T_e and n measured with the Langmuir probe as a function of the angle θ for the three discharge voltages. For clarity reasons the results are only presented at two different distances from the thruster exit plane, 300 and 500 mm respectively.

The cathode potential to ground is very similar for the three operating conditions: $CRP = -14 \pm 1$ V. The mean discharge current is almost the same for a discharge voltage of 150 V and 200 V ($I_d = 3.46$ respectively 3.47 A). For $U_d = 300$ V the mean discharge current is the highest ($I_d = 3.65$ A).

As it can be seen in Figure 4(a), the plasma potential ϕ decreases with the angle θ. For angles smaller than 20 ° the plasma potential increases the higher discharge voltage is. For $\theta > 20$ ° , there is no clear difference for the 3 different operating conditions. The electron temperature T_e also decreases with the angle θ, as shown in Figure 4(b). For $\theta < 30°$, the electron temperature increases for higher discharge voltages, whereas for $\theta > 30°$, there is almost no difference for the 3 different discharge voltages. Figure 4(c) shows that the electron density n decreases with the angle θ. The electron density drops by a factor of 3 for $U_d = 300$ V, respectively by a factor of 2 for $U_d = 200$ V and by a factor of 1.5 for $U_d = 150$ V. Expectedly, all three parameters also decrease with the distance from the thruster exit plane.

III.B. Far-field plume of the PPI thruster

The PPI was operated at a constant anode/cathode mass flow rates of 1.0 mg/s and 0.2 mg/s respectively, with two different discharge voltages (U_d =200 and 225 V). Figure 5 shows ϕ, T_e and n measured with the Langmuir probe at different positions in the far-field plume for the two discharge voltages.

Like with the PPS®100-ML thruster, the cathode potential to ground is very similar for the two operating conditions: $CRP = -18.25 \pm 0.45$ V. The mean discharge current is almost the same for the two different operating conditions: $I_d = 0.93$ A for 200 V and $I_d = 0.92$ A for 225 V.

As can be seen in Figure 5(a), the plasma potential ϕ decreases with the distance from the thruster exit plane and the thruster axis. The plasma potential is significantly higher for the higher discharge voltage. The electron temperature T_e also decreases with the distance from the thruster exit plane and the thruster axis, as shown in Figure 5(b). The electron temperature increases with the discharge voltage. Figure 5(c) shows that the electron density n decreases with the distance from the thruster exit plane and the thruster axis. Again, n is highest for the higher discharge voltage.

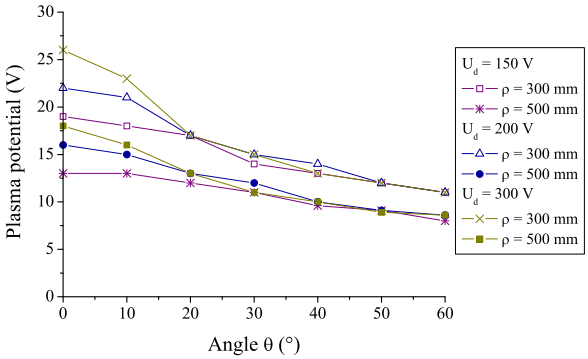

(a) Plasma potential

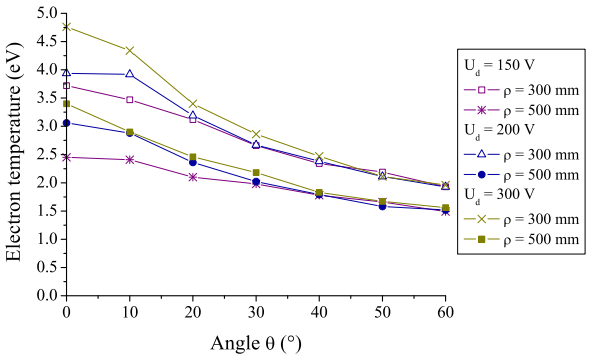

(b) Electron temperature

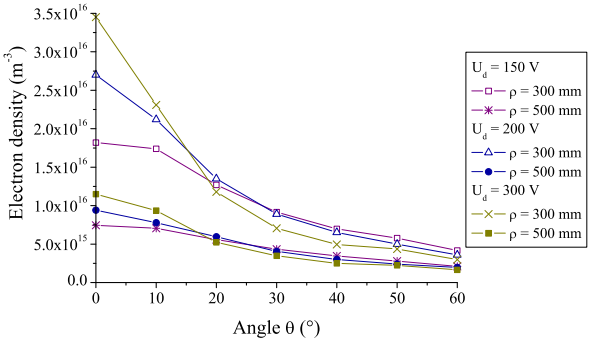

(c) Electron density

Figure 4. Influence of the discharge voltage on the plasma parameters measured in the far-field plume of the PPS®100-ML operating at $\dot{m}_a = 4.0$ mg/s and $\dot{m}_c = 0.42$ mg/s.

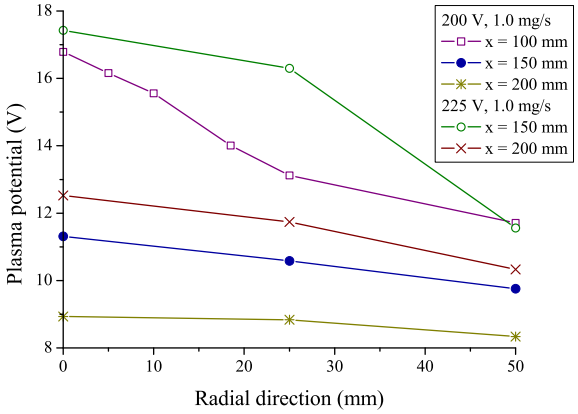

(a) Plasma potential

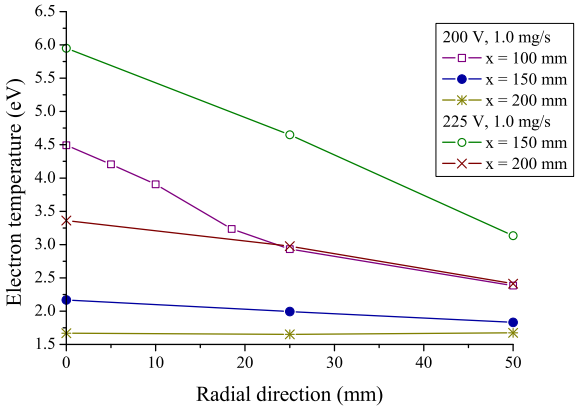

(b) Electron temperature

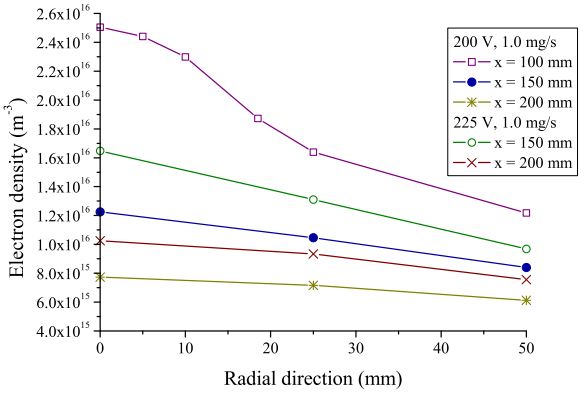

(c) Electron density

Figure 5. Electron properties measured in the far-field plume of the PPI thruster operating at $\dot{m}_a = 1.0\,\mathrm{mg/s}$ and $U_d = 200$ respectively 225 V.

IV. Plume model and fitting of the results

IV.A. Hypersonic plume model

This section summarily reviews a simplified model of the expansion in the plume. A complete derivation of this model and other variants, and the analysis of the error committed by them can be found in Ref. 12 and references cited therein.

The steady state axisymmetric motion of collisionless, fully ionized quasineutral plasma plume expanding into vacuum can be described by the following equations for ions in cylindrical coordinates,

$$u_{xi}\frac{\partial \ln n}{\partial x}+u_{yi}\frac{\partial \ln n}{\partial y}+\frac{\partial u_{xi}}{\partial x}+\frac{1}{y}\frac{\partial \left(yu_{yi}\right)}{\partial y}=0, \tag{1}$$

$$u_{xi}\frac{\partial u_{xi}}{\partial x}+u_{yi}\frac{\partial u_{xi}}{\partial y}+\frac{e}{m_i}\frac{\partial \phi}{\partial x}=0, \tag{2}$$

$$u_{xi}\frac{\partial u_{yi}}{\partial x}+u_{yi}\frac{\partial u_{yi}}{\partial y}+\frac{e}{m_i}\frac{\partial \phi}{\partial y}=0, \tag{3}$$

and the equation of motion for (polytropic) electrons

$$\gamma T_e\nabla \ln n-e\nabla \phi=0, \tag{4}$$

where electron inertia, collisions and currents have been neglected, and $T_e=T_{e0}\left(n/n_0\right)^{\gamma-1}$. The initial section $x=0$ can be placed at any desired location within the far plume. Here, we will place the initial section at the position of the first experimental measurement point (i.e., that of the measurement point closer to the thruster exit section). Subindex 0 denotes the value at $x=y=0$. Initial ion sonic velocity $c_{s0}=\sqrt{\gamma T_{e0}/m_i}$, thruster radius R, and n_0 are used to normalize the equations. The normalized variables are hereon denoted with a hat, e.g. $\hat{u}_{xi}=u_{xi}/c_{s0}$.

A simplified model of these equations can be derived if we assume the hypothesis of self-similar flow, i.e., that all ion streamlines expand likewise, $\hat{y}\left(\hat{x}\right)=\hat{y}\left(0\right)h\left(\hat{x}\right)$, where $h\left(\hat{x}\right)$ (with $h\left(0\right)=1$) is the non-dimensional function, yet to be determined, which provides the shape of the ion streamlines. Ion velocity components are hence related by $\hat{u}_{yi}=\hat{u}_{xi}\hat{y}h'/h$. The new variables $\zeta=\hat{x}$ and $\eta=\hat{y}/h\left(\zeta\right)$ are used in the following. Note that streamlines are given by $\eta=$const. Substitution of ϕ in Eqs. (1)–(3) using Eq. (4) and separation of variables into their streamwise and perpendicular functional dependences,

$$\hat{u}_{xi}\left(\zeta,\eta\right) = u_c\left(\zeta\right)u_t\left(\eta\right), \tag{5}$$

$$\hat{n}\left(\zeta,\eta\right) = n_c\left(\zeta\right)n_t\left(\eta\right), \tag{6}$$

reduces Eqs. (1)–(3) to the following expressions:

$$h^2n_cu_c=M_0, \tag{7}$$

$$u_cu_c'u_t^2+\left(n_cn_t\right)^{\gamma-2}\left(n_c'n_t-n_cn_t'\frac{\eta h'}{h}\right)=0, \tag{8}$$

$$\frac{hu_c\left(u_ch'\right)'}{n_c^{\gamma-1}}=-\frac{n_t^{\gamma-2}n_t'}{\eta u_t^2}=C, \tag{9}$$

with $M_0=u_{c0}$ the initial Mach number, and C a separation constant. It is apparent that Eq. (8) is not separable in the same fashion as Eq. (9), which means that the self-similarity hypothesis and the separation of variables used are *incompatible* with the fluid equations(1)–(4). However, there is a sensible approach to obtain an approximate solution for hypersonic flows in spite of this incompatibility. In a hypersonic ($M\gg 1$) plume, relative variations of axial velocity along the flow direction are small, $\Delta M\sim\Delta\ln n/M$, allowing to neglect Eq. (8) and assume $u_c=$const throughout the plume. In this way, the incompatibility is overcome, at the price of committing an error as noted below.

A second assumption for the evolution of u_t is necessary to close the problem. Different closures have been proposed in the literature that entail choosing a initial u_t or n_t profile based on certain hypotheses.[4,13,14] Here, we follow Korsun et al.,[14] who impose the fulfillment of the derivative on η of Eq. (8), which leads to

$$n_t^{\gamma}=u_t^2. \tag{10}$$

Equations (7), (9) and (10) yield the following solution for n_t,

$$n_t = \left(1 + C\frac{\eta^2}{2}\right)^{-1}, \tag{11}$$

and the h function is determined by

$$h' = \sqrt{h_0'^2 - \frac{C}{M_0^2\,(\gamma-1)}\left(h^{-2(\gamma-1)} - 1\right)}. \tag{12}$$

The purposeful omission of Eq. (8) in the model incurs into a local relative error ε at each ζ, η, which is defined as the left hand side of Eq. (8) divided by $\hat{u}_{xi}^2/R$,

$$\varepsilon\,(\zeta,\eta) = \frac{-2}{M_0^2}\frac{h'}{h^{2\gamma-1}}. \tag{13}$$

This error is proportional to $1/M_0^2$, and therefore arguably small for $M_0 \gg 1$ flows.

The resultant model depends on the Mach number, M_0, the initial slope h_0', the polytropic constant γ, and the separation constant C. This constant is a measure of the radial concentration of the density profile: lower values denote an initially more radially-expanded plume.

IV.B. Fitting to experimental results

The model derived above can be used to fit the experimental results of section III and gain a better understanding of the flow characteristics. For instance, it can be used to obtain the approximate ion streamlines, and to extrapolate the different variables beyond the measurement region. Due to the nature of the model, which assumes a well-established free-plume regime in order to invoke the quasi-selfsimilarity of the fluid equations, upstream extrapolation towards the near-region of the thruster should be considered with care. Using the least-squares (LSQ) method, parameters C, h_0' are fixed by fitting the model to the experimental density data, while γ is fixed using the T_e–n relationship. Due to reduced number and limited spatial extent of the measurements, the Mach number is better fixed from the direct measurements of the velocity (only available for PPI thruster at 225 V), or estimated when no such data is available. An adequate estimate in a HET is to assume that the velocity of ions at the axis is roughly 70% of $\sqrt{2eU_d/m_i}$, the maximum velocity ions would acquire if accelerated by the whole discharge voltage of the thruster. The remaining energy is lost to ionization, excitation, and other loss phenomena.

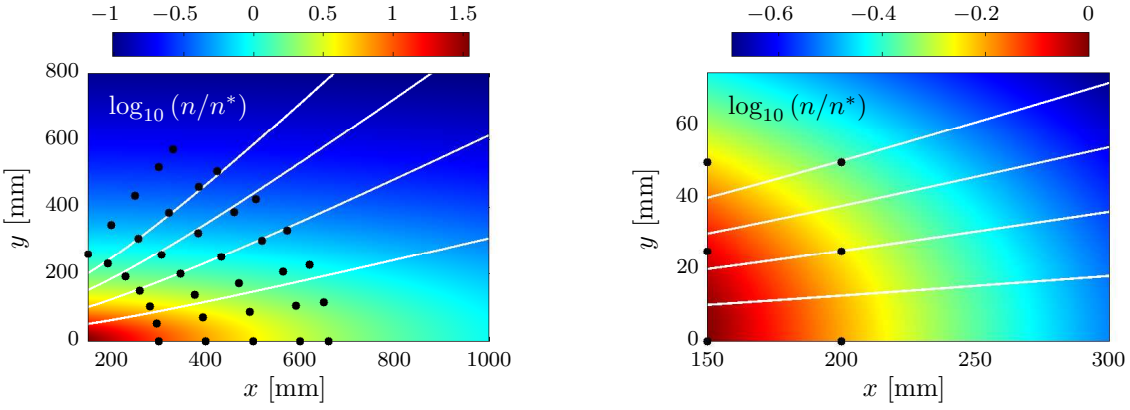

Figure 6. Plasma density maps in the plasma plume of the PPS®100-ML thruster at 300 V (left) and the PPI thruster at 225 V (right). The position of the measurement points is displayed with black dots. Selected ion streamlines are drawn in white. The normalized value presented here is $\log_{10} n/n^*$, where n^* is the density at the first measurement point (i.e., the leftmost measurement point in the figures; $2.98 \cdot 10^{15}$ m^{-3} for the PPS®100-ML, $1.65 \cdot 10^{16}$ m^{-3} for the PPI). The thruster exit section is located at $x = 0$. The model initial section has been located at the position of the first (leftmost) measurement point. Notice that figure is not in 1:1 ratio for practical reasons.

The resulting fitted plume model for two selected cases of section III (PPS®100-ML thruster operating at 300 V and the PPI thruster at 225 V) are presented in Figure 6. The plots show a downstream-extrapolated

region of the flow and ion streamlines as well. The model correctly reproduces the axial and radial density observed experimentally in the plume. The residual pressure causes the plume divergence angle to continue increasing downstream at a very slow pace, as can be observed in the PPS®100-ML case. However, the region of analysis is not large enough for this effect to manifest in the PPI case presented here. Nevertheless, the slow divergence rate allows to approximate ion streamtubes by cones in the region of interest in both cases.

Tables 1 and 2 present a summary of the data fitting for all the experimental cases of section III. Quality of the fit depends on the model error ($\propto 1/M_0^2$), the adequacy of its radial profile to describe the plume of the thruster, and the number and quality of available experimental measurements. The low variance s^2 in all LSQ fittings indicates a great agreement between the model and measured profiles in all cases. The local error of the model, ε, is also sufficiently small for all practical purposes. These two facts support the goodness of the match and the applicability of this method to study the plume of a HET.

Case	M_0	h'_0	γ	C	s^2, $\hat{n}$	s^2, $\hat{T}_e$	$\lvert\varepsilon\rvert_{max}$
300 V	8.93	$4.338{\cdot}10^{-3}$	1.38	$1.001{\cdot}10^{-3}$	$5.561{\cdot}10^{-2}$	$2.856{\cdot}10^{-3}$	$4.627{\cdot}10^{-3}$
200 V	7.58	$3.883{\cdot}10^{-3}$	1.38	$5.818{\cdot}10^{-4}$	$4.926{\cdot}10^{-2}$	$6.241{\cdot}10^{-3}$	$5.743{\cdot}10^{-3}$
150 V	7.38	$3.272{\cdot}10^{-3}$	1.42	$2.855{\cdot}10^{-4}$	$3.438{\cdot}10^{-2}$	$3.755{\cdot}10^{-3}$	$5.106{\cdot}10^{-3}$

Table 1. PPS fitting results. s^2 is the variance (normalized) for the n and T_e LSQ fits, respectively. Mach number was estimated assuming that ions are accelerated to $0.7\sqrt{2eU_d/m_i}$. $\lvert\varepsilon\rvert_{max}$ is the maximum value of the relative local error of the model in the region of experimental data measurements, non-dimensionalized using the thruster radius.

Case	M_0	h'_0	γ	C	s^2, $\hat{n}$	s^2, $\hat{T}_e$	$\lvert\varepsilon\rvert_{max}$
225 V	7.36	$4.94{\cdot}10^{-3}$	2.184	$5.853{\cdot}10^{-4}$	$6.840{\cdot}10^{-4}$	$1.190{\cdot}10^{-4}$	$3.378{\cdot}10^{-3}$
200 V	7.92	$7.45{\cdot}10^{-3}$	1.871	$1.197{\cdot}10^{-3}$	$2.233{\cdot}10^{-3}$	$1.914{\cdot}10^{-3}$	$4.396{\cdot}10^{-3}$

Table 2. PPI fitting results. For the 225 V case, measured u_{xi} was used to calculate the Mach number. For the $U_d = 200$ V case, an ion velocity of $0.7\sqrt{2eU_d/m_i}$ was used to estimate the Mach number. Other variables are as in table 1.

Some of the most remarkable differences between the two thrusters are the higher heat ratio γ (discussed below), and slightly higher flow tangent h'_0 in the PPI thruster, in spite of the similar Mach numbers. However, more experimental data is certainly necessary to confirm the observed tendencies. Due to its importance as a parameter in the development of the plume, the rough approximation used for the ion velocity should also be substituted with Mach number measurements where possible. The more numerous measurements in the PPS®100-ML cases result in a higher fitting variance s^2 for n (although still acceptably small).

In regard with the value of γ found for the PPI thruster, it is significantly higher than the one for the PPS®100-ML. The theoretical maximum value for electrons is $\gamma = 5/3$. However, in a plasma the value of γ can be lower than this value, as an additional degree of freedom is caused by ionization.[15] The high values of γ beyond this limit can be due to measurement inaccuracies and lack of experimental data. It might also be an indication of the presence of some unidentified mechanism that produces additional electron cooling in the plume. However, definitely more experimental data is necessary to clarify its cause.

V. Conclusion

The far-field plume of two different Hall effect thrusters, PPS®100-ML and PPI, was characterized with experimental probe measurements and numerical self-similar fluid models.

The plasma properties (ϕ, T_e and n) were measured by means of a single cylindrical Langmuir probe in the far-field plume for different operating conditions of each thruster. It has been shown that these plasma properties decrease with the distance from the thruster exit plane and the thruster axis as the hypersonic plasma plume expands into the vacuum. A self-similar fluid model of the plasma plume that depends on the Mach number M_0, the initial streamline divergence rate h'_0, the polytropic constant γ, and the initial profile width was used to fit the experimental data. The model has then been used to obtain the flow direction and an downstream extrapolation of the different plasma properties outside the measurement region. Experimental data and numerical models show good agreement.

The presented method provides thus a simple characterization of the plasma plume of Hall effect thrusters, which can be used as a tool for preliminary thruster optimization.

Acknowledgments

The experimental work was carried out in the frame of the CNRS/CNES/SNECMA/Universités joint research program GdR 3161 entitled "*Propulsion par plasma dans l'espace*". Work of the EP2 group was supported by the Gobierno de España (Project AYA-2010-61699).

References

[1]Zhurin, V.V., Kaufmann, H.R., Robinson, R.S., "Physics of closed drift thrusters", Plasma Sources Sci. Technol. **8**, R1-R20, 1999.

[2]Hofer, R.R., Jankovsky, R.S., Gallimore, A.D., "High-specific impluse Hall thrusters, Part 1: Influence of current density and magnetic field", J. Propul. Power **22**, 721-731, 2006.

[3]Darnon, F., "Plume effects in plasma propulsion, An overview of CNES activities", *3rd International Conference on Spacecraft Propulsion (Cannes)*, ESA SP-465, 2000.

[4]Goebel, D.M. and Katz, I., "Fundamentals of electric propulsion: ion and Hall thrusters", John Wiley & Sons, 2008.

[5]Merino, M.; Ahedo, E.; Bombardelli, C.; Urrutxua, H.; Pelaez, J. & Summerer, L., "Space Debris Removal with an Ion Beam Shepherd Satellite: target-plasma interaction", *Proceedings of the 47th AIAA/ASME/SAE/ASEE Joint Propulsion Conference & Exhibit*, AIAA-2011-6142, AIAA, Washington DC, 2011.

[6]Dannenmayer, K., Kudrna, P., Tich, M., Mazouffre, S., "Measurement of plasma parameters in the far-field plume of a Hall effect thruster", Plasma Sources Sci. Technol. **20**, 065012, 2011.

[7]Gascon, N., Dudeck, M., Barral, S., Wall material effects in stationary plasma thrusters I. Parametric studies of an SPT-100, Phys. Plasmas **10**, 4123-4136, 2003.

[8]Leufroy, A., Gibert, T., Bouchoule, A., "Characteristics of a permanent magnet low-power Hall thruster", *31th International Electric Propulsion Conference (Ann Arbor)*, IEPC-2009-083, 2009.

[9]Guyot, M., Renaudin, P., Cagan, V., Boniface, C., patent FR 07 05658, 2007.

[10]Guyot, M. et al., "New Concepts for Magnetic Field Generation in Hall Effect Thrusters", *5th International Spacecraft Propulsion Conference*, Heraklion, Greece, 2008.

[11]Lejeune, A. et al., Impact of the channel width on Hall thruster discharge properties and performances, *32nd International Electric Propulsion Conference (Wiesbaden)*, IEPC-2011-019 (2011).

[12]Merino, M., Ahedo, E., Bombardelli, C., Urrutxua, H., and Peláez, J., "Hypersonic Plasma Plume Expansion in Space," 32^{nd} *International Electric Propulsion Conference*, No. IEPC-2011-086, Electric Rocket Propulsion Society, Fairview Park, OH, 2011.

[13]Ashkenazy, J. and Fruchtman, A., "Plasma Plume Far Field Analysis," *27th International Electric Propulsion Conference*, No. IEPC-01-260, Electric Rocket Propulsion Society, Fairview Park, OH, 2001.

[14]Korsun, A. and Tverdokhlebova, E., "The characteristics of the EP exhaust plume in space," *33rd AIAA/ASME/SAE/ASEE Joint Propulsion Conference & Exhibit*, AIAA, Washington DC, 1997.

[15]Burm, K.T.A.L.; Goedheer, W.J.; D.C. Schram, D.C., "The isentropic exponent in plasmas", Phys. Plasmas **6**, 2622-2627, 1999.